Progress in PHOTOVOLTAICS

PROGRESS IN PHOTOVOLTAICS: RESEARCH AND APPLICATIONS
Prog. Photovolt: Res. Appl. (2016)
Published online in Wiley Online Library (wileyonlinelibrary.com). DOI: 10.1002/pip.2775

RESEARCH ARTICLE

Process development and comparison of various boron emitter technologies for high-efficiency (~21%) n-type silicon solar cells

Kyungsun Ryu[1], Eunhwan Cho[1], Ajeet Rohatgi[1,2] and Young-Woo Ok[1]*

[1] University Center of Excellence for Photovoltaics Research and Education, School of Electrical and Computer Engineering, Georgia Institute of Technology, Atlanta, GA 30332, USA
[2] Suniva Inc., 5765 Peachtree Industrial Blvd., Norcross, GA 30092, USA

ABSTRACT

This paper shows for the first time a comparison of commercial-ready n-type passivated emitter , rear totally diffused solar cells with boron (B) emitters formed by spin-on coating, screen printing, ion implantation, and atmospheric pressure chemical vapor deposition. All the B emitter technologies show nearly same efficiency of ~20%. The optimum front grid design (5 busbars and 100 gridlines), calculated by an analytical modeling, raised the baseline cell efficiency up to 20.5% because of reduced series resistance. Along with the five busbars, rear point contacts formed by laser ablation of dielectric and physical vapor deposition Al metallization resulted in another 0.4% improvement in efficiency. As a result, 20.9% efficient n-type passivated emitter, rear totally diffused cell was achieved in this paper. Copyright © 2016 John Wiley & Sons, Ltd.

KEYWORDS

boron emitter technologies; n-type PERT solar cell; implantation; spin-on boron; screen printing boron paste; APCVD boron source

***Correspondence**

Young-Woo Ok, University Center of Excellence for Photovoltaics Research and Education, School of Electrical and Computer Engineering, Georgia Institute of Technology, Atlanta, GA 30332, USA.
E-mail: yok6@mail.gatech.edu

Accepted 7 March 2016; Received 14 August 2015; Revised 19 February 2016

1. INTRODUCTION

Even though p-type silicon (Si) is widely used in photovoltaic industry today, n-type Si has become an extensive and active research area because of several advantages including no light-induced degradation, high bulk lifetime, and high tolerance to metal impurities [1–3]. P-type Si solar cells are currently used in mainstream solar cell production partly because of cost and technical challenges associated with the formation and passivation of heavily doped boron (B) emitter. Therefore, various B doping technologies are being investigated, but there is no clear winner at this time. The objective of this paper is to fabricate and compare high-efficiency n-type Si solar cells with various promising B diffusion technologies.

BBr_3 diffusion in a tube furnace is one of the most widely used techniques for the B emitter formation. However, it involves hazardous chemical and requires an extra masking step and the mask removal step to form single side B emitter required for Si solar cells. This leads to higher cost and lower throughput for commercialization of n-type solar cell. To overcome the shortcomings of BBr_3 diffusion, several other technologies such as spin-on coating, screen printing, ion implantation, and atmospheric pressure chemical vapor deposition (APCVD) are being explored for the formation of single side B emitters. For example, Das *et al.* [4] and Barth *et al.* [5] reported on 4 cm^2 20.3% and a 241 cm^2 19.3% n-type front junction Cz Si solar cells, using a spin-on boron dopant source. Ryu *et al.* [6] showed a 239 cm^2 19.6% n-type Cz Si solar cell using screen-printed B emitter. Yuguo *et al.* [7] and Boscke *et al.* [8] recently reported on 239 cm^2 20.2 and 20.5% efficient ion-implanted n-type Cz Si solar cells, respectively. Benick *et al.* [9] also reported a 4 cm^2 22.7% fully implanted n-type PERT solar cell. Finally, Rothhardt *et al.* [10] showed a 15.6×15.6 cm^2 19.6% bifacial n-type Cz Si solar cell with B emitter formed by APCVD technique. Notice that previously mentioned reports and investigations used different material, cell design, and process conditions (size, Si material, cell structure, surface

passivation, etc.) that makes it difficult to evaluate and compare different boron emitter technologies and determine which emitter technology is superior and more manufacturable. Furthermore, no systematic study has been conducted to compare these technologies by fabricating commercial-ready n-type solar cells at the same time with the only difference in the B emitter formation. This study shows for the first time a comparison of ~20% efficient baseline n-type passivated emitter, rear totally diffused (PERT) solar cells with B emitters formed by spin-on coating, screen printing, ion implantation, and APCVD while keeping the Si substrate, size, and all other cell processing steps identical.

In addition, using one of the most manufacturable B emitter technologies, advanced n-type PERT solar cells are also fabricated with efficiency target of 21%. This involves technology development, device modeling, front grid design optimization, and formation of rear point contacts by laser ablation of dielectric followed by physical vapor deposition (PVD) of aluminum (Al).

2. EXPERIMENTAL AND RESULTS

2.1. Fabrication of baseline n-type PERT cell using different B technologies

Figure 1 shows the structure and process flow of the baseline n-type PERT cell fabrication using different B emitter technologies. First, both surfaces of 156 × 156 mm pseudo-square 5 Ω cm n-type Cz Si wafers were randomly textured followed by an RCA clean. Then, B source was applied on the entire front surface by either spin-on coating, screen printing, ion implantation, or APCVD technology. Dilute (1 wt%) boric acid (>99.999%, Aldrich Co.) solution was used for the spin-on coating, and Honeywell printable boron source (ACCUPRINT™ B dopant) was used for the screen printing technology. In case of ion implantation, B dopants were implanted with $3 \times 10^{15}\,cm^{-2}$ dose and 10 keV energy on the entire front surface. Finally, for the APCVD emitter technology, borosiligate glass layer capped with undoped SiO_x was deposited on the front side of the Si wafers. After the single side application of B sources, all the samples were annealed at a temperature of 1000 °C for 10 min in a tube furnace in nitrogen (N_2) ambient (the first anneal step). The textured rear side of the wafers was planarized by capping the front side with PECVD silicon nitride (SiN_x) layer and planarizing the back by a diluted potassium hydroxide (KOH) solution, followed by a hydrofluoric acid dip to remove the front SiN_x cap layer. Subsequently, boron-rich layer (BRL) created on the front side after the first annealing step was removed by a chemical etching treatment using a mixture of nitric acid (HNO_3), acetic acid (CH_3COOH), and hydrofluoric acid [11]. The BRL etching time was tailored for each diffusion technology because of the different BRL thickness for different B emitter technologies. Next, phosphorus (P) dopants were implanted with $2.6 \times 10^{15}\,cm^{-2}$ dose and 10 keV energy on the entire planar rear side followed by ~850 °C anneal including *in situ* oxidation to anneal the impalnted P dopants and grow silicon oxide (SiO_2) on both Si surfaces (the second anneal step). Both oxidized surfaces were then capped with PECVD SiN_x layer of appropriate thickness for effective anti-reflection (AR) coating and light trapping. Ag/Al paste was used to screen-print a three busbar grid pattern on the front side, while a dot pattern was screen-printed using a Ag paste on rear side. The wafers were fired in a belt furnace at a peak temperature of ~700 °C for a short period to form the front and back contacts simultaneously through the dielectric stack. Finally, another Ag paste was screen-printed on the entire rear side followed by a short low-temperature drying step to connect the screen-printed Ag dots.

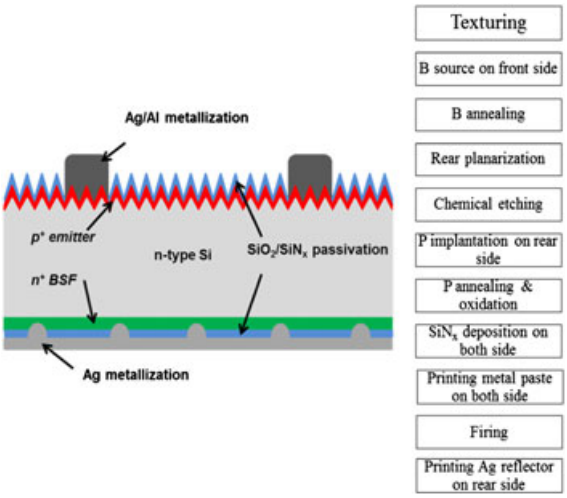

Figure 1. The structure and process flow of n-type PERT cells.

2.2. Comparison of *I–V* results of the baseline n-type PERT cells with different B emitter technology

Table I shows the average and best cell efficiencies of the n-type PERT solar cells fabricated with the four different B emiter technologies: spin-on coating, screen printing, ion implantation, and APCVD. The average efficiency was in the range of 19.9 to 20.1%, and the best efficiency was over 20.0% for all four B technologies. It is noteworthy that no appreciable difference was observed in the cell efficiency of all four technologies. With the exception of ion implantation, these are some of the highest reported efficiencies for large-area n-type PERT Cz Si solar cells with front B emitters formed by spin-on coating, screen printing, and APCVD. These results indicate the potential of all four boron technologies for commercial use up to a baseline cell efficiency of 20%. There were some minor wrap around issues around the edges with the spin-on, screen printing, and APCVD technologies that were resolved by etching during the planarization step. Out of these four B technologies, only ion implantation had no wrap around issues, and

Table I. Summary of *I–V* results of n-type PERT cells with different B technologies.

B formation technology		V_{oc} (mV)	J_{sc} (mA/cm^2)	FF (%)	η (%)
Spin-on coating	Best	648	38.90	79.1	20.0
	Average (no. 8)	648	38.77	79.0	19.9
Screen printing	Best	650	38.77	80.1	20.2
	Average (no. 8)	649	38.50	79.8	20.0
Ion implantation	Best	650	39.23	79.2	20.2
	Average (no. 10)	649	39.11	79.1	20.1
APCVD	Best	652	39.10	79.3	20.2
	Average (no. 10)	649	39.07	79.1	20.0

it also produced highest average baseline cell efficiency. However, cost, throughput, and yield need to be evaluated besides cell efficiency to pick the clear winner, which was difficult to do in this small study.

2.3. Optimization of chemical etching time for each boron technology

In order to find the optimum etching time for each B technology, n-type PERT solar cells with screen-printed B emitters were first fabricated as a function of BRL etching time. Figure 2 shows the efficiency trend for screen-printed B technology. The average cell efficiency increases initially and then decreases, indicating the optimum BRL etching time of 240 s. This optimum is the result of under-etching and over-etching of the BRL. The under-etching of the BRL results in poor surface passivation as well as bulk lifetime degradation after the oxidation step during the second anneal [6,12]. The over-etching starts to thin or shave the B emitter, resulting in lower surface concentration and a decrease in fill factor (FF) and efficiency. The optimum BRL etching was also confirmed by transmission electron microscopy measurement as shown in Figure 2. These transmission electron microscopy images support that 240-s etching time is sufficient and optimum to completely remove the BRL formed on the screen-printed B emitter [13]. This BRL etching process was also optimized for the other B diffusion technologies that showed different optimum etching time for different B technologies (Figure 3). This is attributed to different BRL thickness. In this study, the optimum BRL etching times for spin coating, screen printing, ion implantation, and APCVD were found to be 30, 240, 120, and 180 s, respectively. The corresponding average efficiencies were 19.9, 20.0, 20.1, and 20.0%, respectively. Figure 3 also suggests that the spin-on coating technology forms the thinnest BRL with the least impact of BRL removal on cell efficiency while the screen printing technology developed the thickest BRL and showed maximum positive impact of BRL etching. The pyramid shape and size of textured Si was not altered after chemical etching as reported in a previous paper [11]. Therefore, measured reflectance is very similar before and after etching process. Because the un-etched samples gave lower J_{sc} than BRL-etched

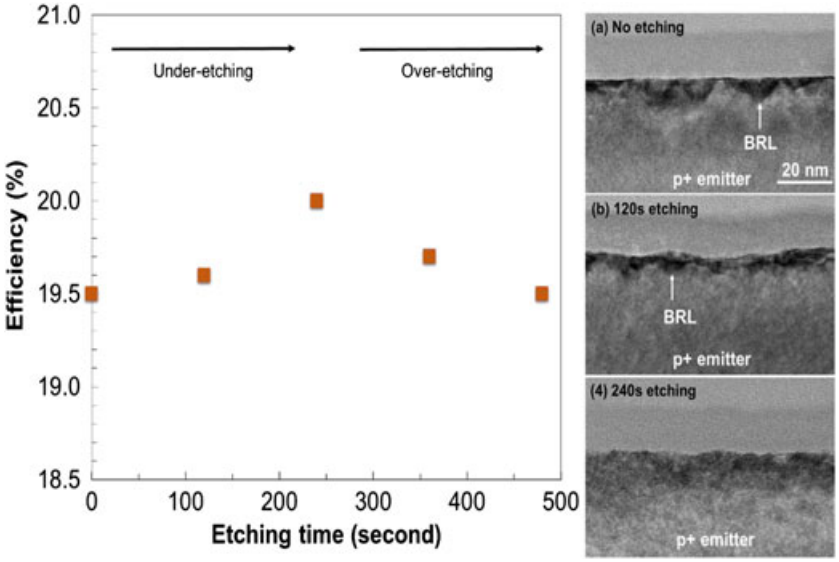

Figure 2. Efficiency trends and transmission electron microscopy images of cross section of screen-printed B emitter as a function of etching time.

DOI: 10.1002/pip

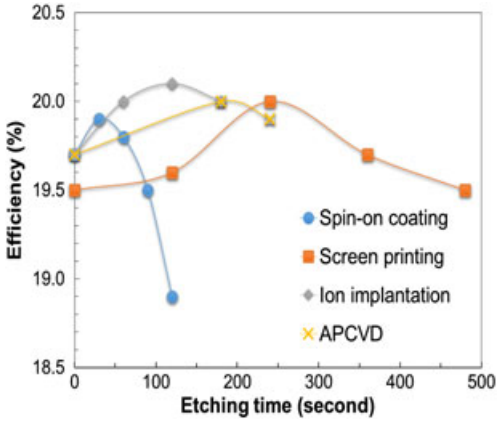

Figure 3. Efficiency trends of four different B technologies as a function of etching time.

samples in spite of same optical properties, BRL layer must act as a source of high recombination.

2.4. 20.5% efficient ion-implanted n-type PERT solar cells with optimized five busbar front grid design

Above baseline, 20% efficient cells were fabricated to compare the different B emitter technologies. In this section, we selected the ion implantation technology to optimize the front and back metal contacts to achieve ~21% efficient large-area (239 cm^2) n-type PERT cells on commercial grade Cz wafers. First, an analytical model for optimizing the front grid pattern was developed in order to reduce series resistance (R_s) and increase FF. The model uses the methodology developed by Meier [14,15] to calculate all the components on R_s from the experimentally determined parameters of the baseline cells. The 20.1% efficient ion-implanted n-type PERT cell was used as the reference. In addition, the model is capable of using the R_s value to calculate cell output parameters such as FF [16], J_{sc}, and V_{oc} [17] and cell efficiency by accounting for resistive and shading associated with grid design including the number of busbars and gridlines. Note that in these calculations, the busbar width was adjusted to keep the same shading of busbars. Thus, total front metal coverage (busbars + fingers) is affected by the number of fingers and not by the number of busbars. The calculated cell efficiency for different grid designs (number of gridlines and busbars) is plotted in Figure 4. The 20.1% efficiency of the reference cell with ~65-μm-wide 90 gridlines and three busbars is in very good agreement with the calculated efficiency that supports the accuracy of this model. Model calculations show that the cell

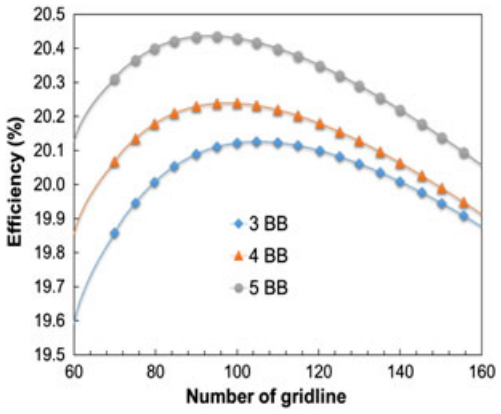

Figure 4. Simulated cell efficiency as a function of number of gridline and busbar.

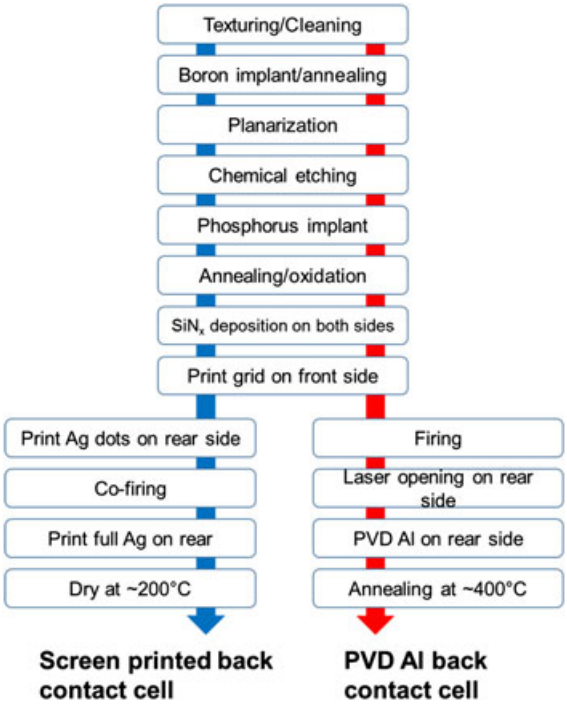

Figure 5. Comparison of process flow for the rear contacts formed by screen-printing and PVD Al.

Table II. *I–V* results of n-type PERT solar cells with three and five busbars.

Front grid design		V_{oc} (mV)	J_{sc} (mA/cm^2)	FF (%)	η (%)	n-factor	R_s (Ω cm^2)	R_{sh} (Ω cm^2)
3 BB, 100 gridlines	Best	652	39.15	79.4	20.3	1.03	0.70	4500
	Average (no. 6)	651	38.88	79.3	20.1	1.04	0.68	9557
5 BB, 100 gridlines	Best	652	38.96	80.8	20.5	1.02	0.47	7010
	Average (no. 8)	652	38.82	80.5	20.4	1.03	0.50	9076

efficiency can be increased from 20.1 to 20.4% simply by increasing the number of busbars from 3 to 5 with 100 gridlines, while keeping the total area of busbars same (0.9-mm-wide five busbars as opposed to 1.5-mm-wide three busbars in the reference cell).

Using the guidelines of this simulation, five busbar cells with 100 gridlines were fabricated and compared with three busbar cells. The same process sequence (Figure 1) was used, and the corresponding *I–V* results are summarized in Table II. The experimental results in Table II are entirely consistent with the model that predicted higher FF and ~0.3% increase in absolute cell efficiency. The three and five busbar cells resulted in an average efficiency of 20.06 and 20.39%, respectively. This improvement is attributed to the reduced series resistance of the front gridlines because of the decrease in the grid length between the busbars.

2.5. ~21% efficient n-PERT cells with five busbars and rear point contacts formed by laser ablation of dielectric and PVD Al metallization

All the previously mentioned n-type PERT cells had 120-μm-wide 500-μm-apart screen-printed Ag metal contacts fired through the rear dielectric stack with metal coverage of 4.5%. This results in higher metal recombination and base saturation current density (J_{0b}). Therefore, in this paper, we replaced the screen-printed dots with much smaller rear point contacts by laser ablation of dielectric followed by the sputtering of Al by PVD. This was accomplished by laser opening 300-μm-apart 40-μm dots. This geometry reduced the metal coverage from ~4.5 to ~1.4% [18].

Figure 5 shows the comparison of process flow for the rear contact formation by screen-printing of Ag dots and PVD Al metallization. Notice that PVD Al metallization process involved screen-printed Ag/Al grid formation on the front first. Then, the rear SiO_2/SiN_x passivation stack was opened to form the 40-μm dot pattern with 300-μm spacing using a UV laser. After that, approximately ~1-μm-thick Al film was sputtered by the PVD Al coated on the entire rear side. Finally, the PVD cells received a short annealing at a temperature of ~400 °C in a belt furnace to achieve a good ohmic contact on the rear side.

Table III shows that compared with the n-type PERT cells with screen-printed rear point contacts (Table II), an improvement of 0.3% in absolute efficiency was achieved for cells with laser ablation and PVD Al metallization. The data also supports that reduced metal-induced recombination on the rear side resulted in ~7 mV increase in V_{oc}. Because the reduced recombination on the rear side reduces back surface recombination velocity, it also gives a slightly higher long wavelength internal quantum efficiency (IQE) response [18], resulting in a slight increase in J_{sc}. Furthermore, PVD Al contact gave slightly higher FF, which is attributed to the combination of reduced n-factor and improved V_{oc} [16]. These improvements resulted in best cell efficiency of 20.9% with a V_{oc} of 659 mV, J_{sc} of 39.05 mA/cm^2, and FF of 81.0%.

Table III. *I–V* results of n-type PERT cell with PVD Al rear contact.

	V_{oc} (mV)	J_{sc} (mA/cm^2)	FF (%)	η (%)	n-factor	R_s (Ω cm^2)	R_{sh} (Ω cm^2)
Best	659	39.05	81.0	20.9	0.99	0.51	4260
Average (no. 7)	658	38.97	80.9	20.8	1.01	0.50	6763

Table IV. PC1D modeling of n-type PERT cells (baseline, five busbar, and PVD Al).

Parameters	Baseline	Five busbars	Five busbars + PVD Al metallization
Thickness (mm)	180	180	180
Base doping (cm^{-3})	9.2×10^{14}	9.2×10^{14}	9.2×10^{14}
Emitter surface concentration (cm^{-3})	4.0×10^{19}	4.0×10^{19}	4.0×10^{19}
Junction depth (mm)	0.65	0.65	0.65
R_s (Ω cm^2)	0.7	0.47	0.50
Bulk lifetime (ms)	~1	~1	~1.5
Front metal coverage (%)	7.5	7.5	7.5
Back metal coverage (%)	4.5	4.5	1.4
FSRV (cm/s)	6000	6000	6000
BSRV (cm/s)	22	22	14
J_{0e} (fA/cm^2)	155	155	155
J_{0b} (fA/cm^2)	295	295	195
Modeled V_{oc} (mV)	652	652	660
Modeled J_{sc} (mA/cm^2)	39.2	39.2	39.2
Modeled FF (%)	79.0	80.2	80.4
Modeled η (%)	20.2	20.5	20.8
Measured V_{oc} (mV)	652	652	659
Measured J_{sc} (fA/cm^2)	39.2	39.0	39.1
Measured FF (%)	79.4	80.8	81.0
Measured η (%)	20.3	20.5	20.9

2.6. Characterization modeling and analysis of n-type PERT cells

Previously mentioned n-type cells were extensively characterized and modeled using PC1D to gain deeper insight into the efficiency enhancements. Table IV summarizes measured and extracted input parameters of the best cell in each category ranging from 20.3% baseline cell to 20.9% advanced cell. Note that 20.5% cell was achieved by replacing three busbars by five busbars while maintaining the same metal coverage and gridlines. This reduced the grid length between the busbar and lowered R_s from 0.70 to 0.47 $\Omega\,cm^2$, resulting in an increase in FF from 79.4 to 80.8%. The 20.9% cell involved back contacts with 300-μm-apart 40-μm dot, which was accomplished by laser ablation and PVD Al metallization. This reduced the metal/Si contact coverage from 4.5 to 1.4%, which, in turn, lowered effective BSRV from 22 to 14 cm/s. Notice that the extracted bulk lifetime improved from 1 to 1.5 ms in the 20.9% device. The reduced BSRV and increased bulk lifetime lowered the J_{0b} [17] from 295 to 195 fA/cm^2 and increased V_{oc} from 652 to 659 mV. Excellent agreement was achieved in between the measured and modeled *I–V* parameters.

3. CONCLUSIONS

In this study, spin-on coating, screen printing, ion implantation, and APCVD technologies were utilized for the B emitter formation. The etching process for the BRL removal was optimized for each B technology. For the 1000 °C B anneal process used in this study, the optimized BRL etching times for spin coating, screen printing, implantation, and APCVD technologies were 30, 240, 120, and 180 s, respectively. The corresponding best baseline efficiencies were 20.0, 20.2, 20.2, and 20.2%. This result shows nearly same efficiency potential of the four B diffusion technologies for basic high-efficiency commercial-ready n-type PERT solar cells with efficiency of ~20%.

The front grid pattern was optimized for the ion-implanted cells using an analytical model, which revealed that five busbars with 100 gridlines can provide 0.3% increase in absolute efficiency compared with the baseline three busbar cells with 100 gridlines. This was validated by fabricating ion-implanted n-type PERT solar cells with five busbar and 100 gridlines that raised the n-type PERT best cell efficiency from 20.3 to 20.5%. This is attributed to reduced R_s because of the decrease in busbar-to-busbar resistance. In addition, back contacts were also optimized by replacing 120-μm-wide 500-μm-apart screen-printed dots with 300-μm-apart 40-μm dots formed by laser ablation and PVD Al metallization. This reduced the back metal/Si contact area from 4.5 to 1.4%, resulting in another 0.4% increase in efficiency. As a result, a best cell efficiency of 20.9% was achieved with V_{oc} of 659 mV, J_{sc} of 39.05 mA/cm^2, and FF of 81.0% for ion-implanted cells.

REFERENCES

1. Schmidt J, Aberle AG, Hezel R. Investigation of carrier lifetime instabilities in Cz-grown silicon. *26th IEEE PVSC Photovoltaic Specialists Conference*, 1997; 13–18.
2. Glunz SW, Rein S, Lee JY, Warta W. Minority carrier lifetime degradation in boron-doped Czochralski silicon. *Journal of Applied Physics* 2001; **90**: 2397–2404.
3. Macdonald D, Geerligs LJ. Recombination activity of interstitial iron and other transition metal point defects in p- and n-type crystalline silicon. *Applied Physics Letters* 2004; **85**: 4061–4063.
4. Das A, Ryu K, Rohatgi A. 20% Efficient screen-printed n-type solar cells using a spin-on source and thermal oxide/silicon nitride passivation. *IEEE Journal of Photovoltaics* 2011; **1**: 146–152.
5. Barth S, Doll O, Koehler I, Neckermann K, Blech M, Lawerenz A, Edler A, Kopecek R, Schneider J. 19.4 Efficient bifacial solar cell with spin-on boron diffusion. *Energy Procedia* 2013; **38**: 410–415.
6. Ryu K, Upadhyaya A, Upadhyaya V, Rohatgi A, Ok Y-W. High efficiency large area n-type front junction silicon solar cells with boron emitter formed by screen printing technology. *Progress in Photovoltaics: Research and Applications* 2015; **23**: 119–123.
7. Tao Y, Ok Y-W, Zimbardi F, Upadhyaya A, Lai J-H, Ning S, Upadhyaya V, Rohatgi A. Fully ion-implanted and screen-printed 20.2% efficient front junction silicon cells on 239 cm2 n-type CZ substrate. *s. IEEE Journal of Photovoltaic* 2014; **4**: 58–63.
8. Boscke T, Kania D, Schollhorn C, Stichtenoth D, Helbig A, Sadler P, Braun M, Dupke M, Weiß M, Grohe A, Lossen J, Krokoszinski H. Fully ion implanted and coactivated industrial n-type cells with 20.5% efficiency. *IEEE Journal of Photovoltaics* 2014; **4**: 48–51.
9. Benick J, Steinhauser B, Muller R, Bartsch J, Kamp M, Mondon A, Richter A, Hermle M, Glunz S. High efficiency n-type PERT and PERL solar cells. *40th IEEE PVSC* 2014; 3637–3640.
10. Rothhardt P, Meier S, Maier S, Jiang K, Wolf A, Biro D. Characterization of POCl-based codiffusion processes for bifacial n-type solar cells. *IEEE Journal of Photovoltaics* 2014; **4**: 827–833.
11. Ryu K, Upadhyaya A, Song HJ, Choi CJ, Rohatgi A, Ok YW. Chemical etching of boron-rich layer and its impact on high efficiency n-type silicon solar cells. *Applied Physics Letters* 2012; **101**: 073902-4: .
12. Sieu Pheng P, Wensheng L, Wolpensinger B, Kessler MA, Macdonald D. Tradeoffs between impurity gettering, bulk degradation, and surface passivation of boron-rich layers on silicon solar cells. *IEEE Journal of Photovoltaics* 2013; **3**: 261–266.

13. Ryu K, Choi C-J, Park H, Kim D, Rohatgi A, Ok Y-W. Fundamental understanding, impact, and removal of boron-rich layer on n-type silicon solar cells. *Solar Energy Materials and Solar Cells* 2015; **146**: 58–62.
14. Meier DL, Chandrasekaran V, Gupta A, Yelundur V, Rohatgi A. Silver contact grid: inferred contact resistivity and cost minimization in 19% silicon solar cells. *IEEE Journal of Photovoltaics* 2013; **3**: 199–205.
15. Meier D, Good E, Garcia R, Bingham B, Yamanaka S, Chandrasekaran V, Bucher C. Determining components of series resistance from measurements on a finished cell. I*EEE 4th World Conference*, 2006; 1315–1318.
16. Green MA. Accuracy of analytical expressions for solar cell fill factors. *Solar Cells* 1982; **7**: 337–340.
17. Ok Y-W, Upadhyaya AD, Tao Y, Zimbardi F, Ryu K, Kang M-H, Rohatgi A. Ion-implanted and screen-printed large area 20% efficient N-type front junction Si solar cells. *Solar Energy Materials and Solar Cells* 2014; **123**: 92–96.
18. Tao Y, Payne A, Upadhyaya VD, Rohatgi A. 20.7% efficient ion-implanted large area n-type front junction silicon solar cells with rear point contacts formed by laser opening and physical vapor deposition. *Progress in Photovoltaics: Research and Applications* 2014; **22**: 1030–1039.

DOI: 10.1002/pip